Transmission channels for light in absorbing random media: From diffusive to ballistic-like transport

Seng Fatt Liew,[1] Sébastien M. Popoff,[1] Allard P. Mosk,[2] Willem L. Vos,[2] and Hui Cao[1,*]

[1]*Applied Physics Department, Yale University, New Haven, Connecticut 06520, USA*

[2]*Complex Photonic Systems (COPS), $MESA^+$ Institute for Nanotechnology, University of Twente, P.O. Box 217, 7500 AE Enschede, The Netherlands*

While the absorption of light is ubiquitous in nature and in applications, the question remains how absorption modifies the transmission channels in random media. We present a numerical study on the effects of optical absorption on the maximal transmission and minimal reflection channels in a two-dimensional disordered waveguide. In the weak absorption regime, where the system length is less than the diffusive absorption length, the maximal transmission channel is dominated by diffusive transport and it is equivalent to the minimal reflection channel. Its frequency bandwidth is determined by the underlying quasimode width. However, when the absorption is strong, light transport in the maximal transmission channel undergoes a sharp transition and exhibits ballistic-like transport. Its frequency bandwidth increases with absorption, and the exact scaling varies with the sample's realization. The minimal reflection channel becomes different from the maximal transmission channel and becomes dominated by absorption. Counterintuitively, we observe in some samples that the minimum reflection eigenvalue increases with absorption. Our results show that strong absorption turns open channels in random media from diffusive to ballistic-like transport.

PACS number(s): 05.60.−k, 42.25.Dd, 73.23.−b

I. INTRODUCTION

In mesoscopic transport, wave interference plays an essential role, giving rise to well-known phenomena such as enhanced backscattering, Anderson localization, and universal conductance fluctuations [1–6]. Recently, another striking interference effect has caught much attention, that is, the existence of highly transmitting channels, termed "open channel" in a random system [7–14]. These open channels, which enable an optimally prepared coherent input beam to transmit through a strong scattering medium with order unity efficiency, were predicted initially for electrons [15–18]. However, they have not been directly observed in mesoscopic electronics due to the extreme difficulty of controlling the input electron states. In contrast, it is much easier to prepare the input states of classical waves, such as electromagnetic waves or acoustic waves. Recent developments of adaptive wavefront shaping and phase recording techniques in optics have enabled experimental studies of open channels [19–22]. The open channels greatly enhance light penetration into scattering media, which will have a profound impact in a wide range of applications from biomedical imaging and laser surgery to photovoltaics and energy-efficient ambient lighting [22–24].

The transmission channels are eigenvectors of the matrix $t^\dagger t$, where t is the field transmission matrix of the system. The eigenvalues τ are the transmittance of the corresponding eigenchannels. In the lossless diffusion regime, the density of eigenvalues τ has a bimodal distribution, with one peak at $\tau \simeq 0$ that corresponds to closed channels, and a peak at $\tau \simeq 1$ that corresponds to open channels [15–18]. The diffusion process is dominated by the open channels, and the average

transmittance is proportional to the ratio of the number of open channels by the total number of propagating channels [15,16]. At the transition to localization, the number of open channels is reduced to one, and the open channels disappear in the localization regime. The conductance of a localized system is dominated by the single highest transmitting channel. In the past few years, wavefront shaping has been utilized to increase the coupling of the incident light to the open channels of random media [7,11,12,14,25,26]. Numerical simulations reveal that the open channels enhance the energy stored inside the disordered medium [9]. In the diffusion regime, the field energy of an open channel is spread over the entire transverse extent of a sample, while in the localization regime the maximal transmission channel becomes confined in the transverse direction normal to the transmission direction [10].

In addition to the transmission channels, the transport can also be interpreted in terms of resonances, which are referred to as "levels" for electrons and "modes" for classical waves [27,28]. For an open system, one can define the quasinormal modes. These are eigenfunctions of the Maxwell equations with complex frequency that satisfy the boundary conditions of the outgoing wave. They describe states that have stationary normalized spatial profiles and amplitudes decaying in time due to radiative losses. These quasinormal modes play an important role in transport, e.g., in the localization regime energy is transported either by tunneling through a localized mode in the middle of the sample or by hopping over a necklace state that is formed via coupling of several localized modes [29–34]. If the input beam is coupled to multiple modes, the interference of these modes at the output end determines the total transmission [27]. Transmission channels and resonant modes complement each other as approaches to describe transport phenomena [28]. At any frequency, the transmission eigenchannels can be expressed as a frequency-dependent superposition of resonant modes with

_____

*[*]hui.cao@yale.edu

specific resonance frequencies and widths. In the localization regime, the maximal transmission channel can typically be identified with a single resonant mode [28].

Absorption of radiation is usually assumed to suppress interference effects such as the occurrence of open channels. Most studies on transmission eigenchannels have considered lossless random media where absorption is negligible. In reality absorption exists in any material system, and could have a significant impact on diffusion and localization [35,36]. In the microwave regime, for instance, absorption is particularly difficult to avoid and leads to a significant reduction of the transmission through disordered waveguides [11,37]. Absorption does not destroy the phase coherence of scattered waves, but it attenuates the longer scattering paths more than the shorter paths, thus modifying the interference patterns. Since the open channels penetrate deeper into the random medium than the closed channels, they would experience more absorption. In other words, absorption should have a stronger effect on the open channels than on the closed channels. However, it is not clear how absorption would modify the open channels. Moreover, it has been shown lately that light absorption in strongly scattering media can be greatly enhanced or inhibited by coherent effects [38–40]. Thus the interplay between absorption and interference determines not only the amount of energy being transmitted, but also the amount of energy being deposited in the random media. The investigation of strongly scattering systems with absorption is therefore not only important to the fundamental study of mesoscopic transport, but also relevant for applications in imaging, light harvesting, and lighting technology [22–24,41,42].

In this paper, we address the following questions: how does absorption modify the open channels? How does the channel bandwidth vary with absorption? What is the correlation between a transmission and a reflection channel in the presence of absorption? In weak absorption, when the ballistic absorption length l_a is much larger than the average path length $l_p = 2L^2/l_t$ (l_t is the transport mean free path), most scattering paths are not affected by absorption. However, when ballistic absorption length becomes smaller than the average path length $l_a < l_p$, attenuation of long scattering paths significantly affects the transport through the system. To study the change of light transport, we compute the spatial field distribution inside the random medium. The spectral width of the maximal transmission channel is important to many of the aforementioned applications, for instance, a broad spectral width is desired for light harvesting. To address this question, we calculate the frequency bandwidth of input wavefront corresponding to the maximal transmission channel and its scaling with absorption. Experimental studies of the transmission channels rely on the access to both sides of the scattering media. It is, however, often more convenient and less invasive to work in a reflection configuration, where all measurements are on the input side of the sample. For example, without absorption, the total transmission is maximized by finding the minimal reflection channel [43]. In the presence of absorption, the relation between the maximal transmission channels and the minimal reflection channels is not known. Therefore, we investigate the correlation between these two channels as a function of absorption.

This paper is organized as follows. In Sec. II, we present our numerical model of two-dimensional (2D) disordered waveguides. In Sec. III we show how absorption modifies the maximal transmission channel and we illustrate its correlation with the quasinormal modes. In Sec. IV, we investigate the minimal reflection channel in the absorbing random media. Section V is the conclusion.

II. NUMERICAL MODEL

We consider a 2D disordered waveguide, shown schematically in Fig. 1. Dielectric cylinders with refractive index $n = 2.5$ and radius $r_c = 0.098\lambda$ are randomly positioned inside the waveguide with perfectly reflecting sidewalls. The dielectric cylinders occupy an area fraction of 0.04 corresponding to an average distance between cylinders of $a = 0.87\lambda$. We select to work at the wavelength of input light that avoids the Mie resonances of individual dielectric cylinders. This frequency is in the photonic regime above the first band gap of a triangular lattice with the same area fraction [44]. Light enters the waveguide from the left open end and is scattered by the cylinders. Light transmitted through or reflected from the random array is absorbed by the perfectly matched layers placed at both ends of the waveguide. We consider transverse-magnetic (TM) polarized light, whose electric field is parallel to the cylinder axis (z axis). The width of the waveguide is $W = 10.3\lambda$; the number of guided modes in the empty waveguide is $N = 2W/\lambda = 20$. The length of the random array of cylinders is $L = 20.2\lambda$.

To calculate the electromagnetic field inside the random waveguide, we solve Maxwell's equations using the finite-difference frequency-domain method [45]. The intensity is averaged over a cross section of the waveguide to obtain the evolution $I(x)$ along the waveguide in the x direction. The ensemble-averaged $I(x)$ exhibits the well-known linear decay, from which we extract the transport mean free path $l_t = 0.073L$ [46]. Since $l_t \ll L$, light experiences multiple scattering. The localization length is $\xi = (\pi/2)Nl_t = 2.3L$. The system is in the diffusion regime, as confirmed from the linear decay of intensity but it is close to the localization regime. The reason we chose this regime is as follows. In the
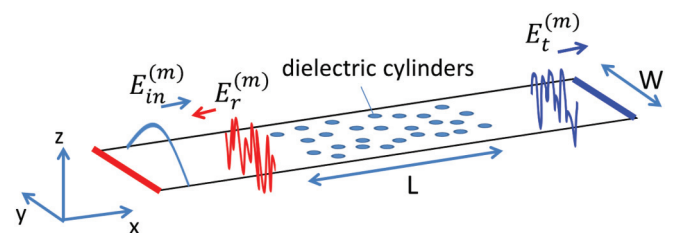

FIG. 1. (Color online) Schematic of the 2D disordered waveguide used in our numerical simulation. Dielectric cylinders are placed randomly in a waveguide with perfect-reflecting sidewalls. The waveguide width is W, and the length of the disordered region is L. A light field $E_{in}^{(m)}$ is launched from the left end of the waveguide, and scattered by the cylinders. The transmitted light field $E_t^{(m)}$ is probed at the right end, and the reflected light field $E_r^{(m)}$ at the left end. Perfectly matched layers are placed at both open ends to absorb the transmitted and reflected waves.

localization regime, the maximal transmission eigenchannel is composed of only one or two quasinormal modes [28]. In the diffusion regime ($\xi \gg L$), many overlapping modes contribute to the maximal transmission channel, making the analysis complicated. Since our system is in the diffusive regime, close to the localization transition, the maximal transmission channel consists of a few quasinormal modes. In this regime the transport displays a large fluctuation from one realization to another. Within the same statistical ensemble there are random realizations that are closer to or further away from the localization transition. We can therefore study a wide range of behavior in the same ensemble.

Usually, absorption exists either inside the scattering particles, in the waveguide wall or in the background material that hosts the particles. The concomitant contrast in the imaginary part of the refractive index causes additional scattering, which modifies the resonant modes [47]. In this paper we prefer to avoid this additional scattering effect by introducing a spatially homogeneous imaginary refractive index γ to both scatterers and background, so that mode wave functions do not change and we can focus on the effects of absorption and energy loss. The ballistic absorption length is $l_a = 1/(2k\gamma)$, where the wave vector is $k = 2\pi/\lambda$. When the ballistic absorption length l_a reaches the average path length of light in a 2D diffusive system $l_p = 2L^2/l_t$, the diffusive absorption length $\xi_a = \sqrt{l_t l_a/2}$ becomes equal to the system length $\xi_a = L$.

To construct the transmission matrix t of the disordered waveguide, we use the guided modes or propagation channels in the empty waveguide as the basis. We launch a guided mode $E_{\text{in}}^{(m)}$ from the input end, calculate the transmitted wave, and decompose it by the empty waveguide modes at the output end, $E_t^{(m)} = \sum_{n=1}^{N} t_{nm} E_{\text{in}}^{(m)}$. The coefficient t_{nm} relates the field transmission from an input channel m to an output channel n. After repeating this procedure for $m = 1, 2, \ldots N$, we obtain all the elements t_{nm} for the transmission matrix t. Similarly, the reflection matrix is constructed by computing the reflected waves $E_r^{(m)}$ at the input end.

III. MAXIMAL TRANSMISSION CHANNEL

A singular value decomposition of the transmission matrix t gives

$$t = U \Sigma V^\dagger, \tag{1}$$

where Σ is a diagonal matrix with non-negative real numbers, $\sigma_n = \sqrt{\tau_n}$, τ_n is the eigenvalue of $t^\dagger t$, $\tau_1 > \tau_2 > \tau_3 \ldots > \tau_N$. U and V are $N \times N$ unitary matrix, V maps input channels of the empty waveguide to eigenchannels of the disordered waveguide, and U maps eigenchannels to output channels. The column vectors in V (U) are orthonormal and are called input (output) singular vectors. The value τ_n represents the transmittance of the nth transmission channel. The input singular
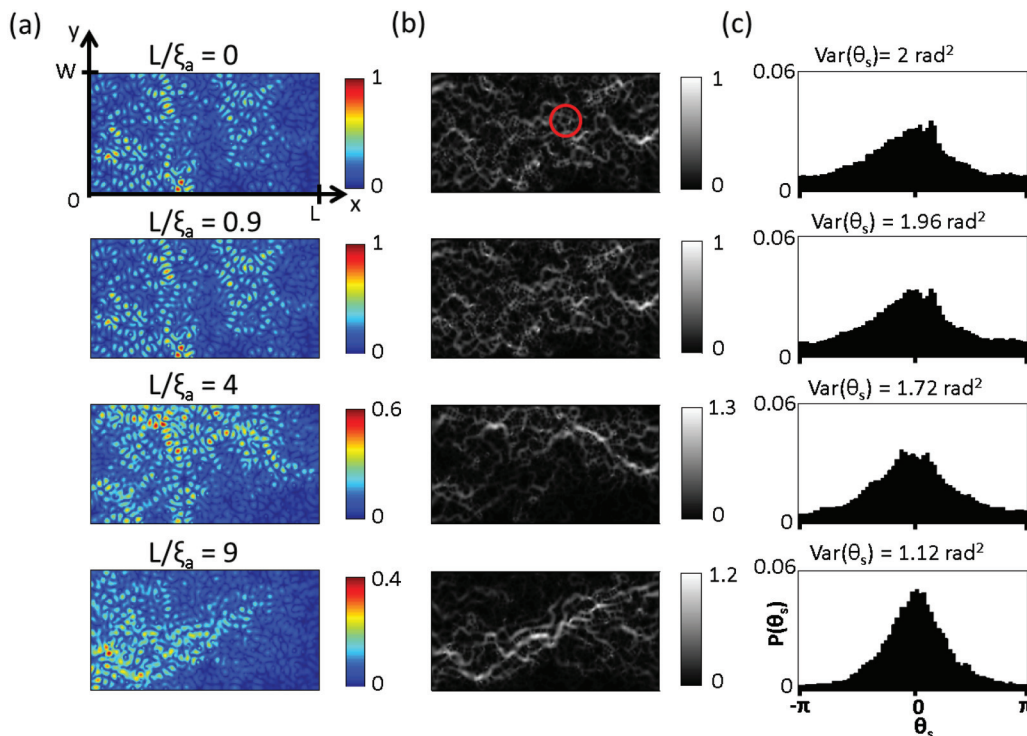

FIG. 2. (Color) Evolution of maximal transmission channel with absorption. Calculated electric field amplitude $|E_z|$ (a), normalized Poynting vector amplitude $|\vec{S}'(x,y)|$ in gray scale (b), and histogram of the weighted Poynting vector direction $P(\theta_s)$ (c) of the maximal transmission channel inside the disordered waveguide as absorption L/ξ_a increases from top to bottom. In (a), the maximal transmission channel remains robust against absorption with a nearly identical field pattern up to $L = \xi_a$ and changes significantly beyond that point. In (b) the winding paths of light are illustrated inside the random structure in the weak absorption regime $L/\xi_a < 1$, and more straight "snake-like" paths in the strong absorption regime $L/\xi_a > 1$. A "loop" in the energy flow is circled in red. In (c), the angle θ_s from the Poynting vector to the x axis is widely spread between $-\pi$ and π when $L/\xi_a < 1$, but concentrates close to 0 when $L/\xi_a > 1$. The variance of θ_s, indicated above each panel, decreases with increasing L/ξ_a

vector corresponding to the highest transmission eigenvalue τ_1 gives the maximal transmission eigenchannel; its elements represent the complex coefficients of the waveguide modes that combine to achieve maximum transmission through the random medium.

A. Effects of absorption on spatial field distribution and energy flow of the maximal transmission channel

We inject light into the maximal transmission channel and investigate the field profile inside the random medium. In Fig. 2(a) we plot the spatial distribution of the electric field amplitude $|E_z|$ inside the disordered waveguide with increasing L/ξ_a. To map the energy flow inside the disordered medium, we compute the Poynting vector $\vec{S}(x,y) = \frac{1}{2}\mathrm{Re}[\vec{E}(x,y) \times \vec{H}^*(x,y)]$. Its projection onto the propagation direction (x axis) is $S_x(x,y) = \vec{S}(x,y) \cdot \vec{e}_x$, where $\vec{e}_x$ is the unit vector along the x axis. The net flow over a cross section of the disordered waveguide is $F(x) = \int_0^W S_x(x,y)dy$. Without absorption, the net flow is a constant, $F(x) = F(0)$. In the presence of absorption, $F(x)$ decays exponentially along x. For a clear visualization of the energy flow deep inside the random structure, we normalize the Poynting vector $\vec{S}(x,y)$ by $F(x)$ to compensate the energy decay such that $\vec{S}'(x,y) = \vec{S}(x,y)/F(x)$. Figure 2(b) plots the magnitude of the normalized Poynting vector $|\vec{S}'(x,y)|$. For a quantitative analysis of the light propagation direction, we compute the angle of the Poynting vector $\vec{S}(x,y)$ with respect to the x axis, $\theta_s(x,y) = \tan^{-1}[(\vec{S}(x,y) \cdot \vec{e}_y)/(\vec{S}(x,y) \cdot \vec{e}_x)]$ where $\vec{e}_y$ is the unit vector along the y axis. In Fig. 2(c), we plot the histogram of θ_s weighted by the relative amplitude of the Poynting vector, $P(\theta_s) = \int |\vec{S}'(x,y)|\delta(\theta_s - \theta_s(x,y))dxdy$.

Let us now discuss the results in Figs. 2(a)–2(c). When absorption is weak ($L/\xi_a < 1$), the maximal transmission channel has nearly the same field pattern as the channel without absorption. The energy flow inside the random structure resembles meandering random paths that are intertwined, and many "loops" are seen. The multiply scattered light propagates in many directions, and the distribution of the Poynting vector's angle $P(\theta_s)$ is broad and has a large variance. Once L/ξ_a exceeds 1, the spatial profile evolves. At $L/\xi_a = 4$, a noticeable change of the field pattern is observed: The loops gradually disappear, and the creeks become straighter. This behavior occurs because the longer scattering paths that involve more windings are strongly attenuated by absorption. To maximize the transmission through the random system, light takes a shorter and more straight path to minimize absorption. As a result, the distribution of the Poynting vector's angle $P(\theta_s)$ becomes narrow and its variance decreases. When absorption becomes very strong ($L/\xi_a = 9$), the maximal transmission channel bears no resemblance to the one with weak absorption. All meandering creeks eventually merge into a single stream with few windings and light propagates mostly in the forward direction.

For a quantitative characterization of the change of the maximal transmission channel by absorption, we compute the correlation of its input singular vector $\mathbf{v_1}$ with the one without absorption $\mathbf{v_0}$:

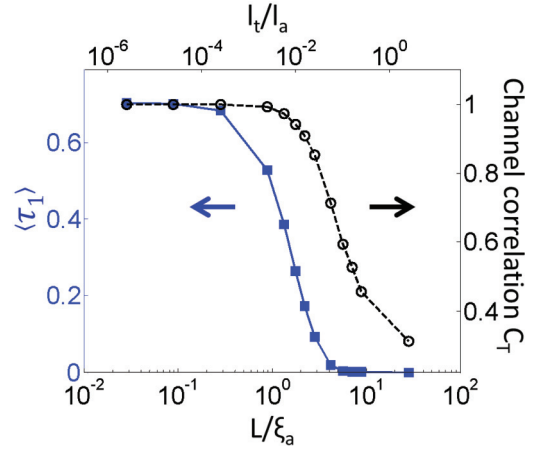$$C_T = |(\mathbf{v_0}, \mathbf{v_1})|, \qquad (2)$$

FIG. 3. (Color online) Maximal transmission eigenvalue and eigenvector vs absorption. Solid squares connected by solid line represent the ensemble-averaged highest transmission eigenvalue $\langle\tau_1\rangle$ as a function of absorption (bottom axis L/ξ_a, top axis l_t/l_a). Open circles connected by dashed line represent the correlation of the input singular vector with absorption to the one without absorption C_T. The maximal transmission eigenchannel changes at a higher absorption level compared to its eigenvalue.

where $(\mathbf{v_0}, \mathbf{v_1}) = \mathbf{v_0}^\dagger \mathbf{v_1}$ is the inner product of the normalized singular vectors $\mathbf{v_1}$ and $\mathbf{v_0}$. Figure 3 plots the channel's correlation C_T, averaged over 40 random realizations, as a function of L/ξ_a. Its value stays close to 1 when the system length is smaller than the diffusive absorption length $L < \xi_a$, and it drops abruptly as $L > \xi_a$. In the same figure, we also plot the ensemble-averaged highest transmission eigenvalue $\langle\tau_1\rangle$ vs L/ξ_a. Due to the small number of input channels ($N = 20$) in the waveguide, the highest transmission eigenvalue $\langle\tau_1\rangle$ does not reach 1 even without absorption ($L/\xi_a = 0$). As the absorption L/ξ_a increases, the highest transmission eigenvalue $\langle\tau_1\rangle$ decreases much earlier than the channel's correlation C_T. For example, at $L/\xi_a = 2.2$, the highest transmission eigenvalue $\langle\tau_1\rangle$ is already reduced by a factor of 4, while the correlation C_T remains more than 0.9. Thus in the weak absorption regime, the maximal transmission eigenvalue decreases while the eigenvector remains almost the same. This means that interference remains strong, and absorption merely reduces the amount of energy reaching the output end, but does not change the interference pattern. However, in the strong absorption regime, the number of significant scattering paths is greatly reduced, and the interference effects are weakened. Consequently, the maximal transmission channel starts to change dramatically and becomes "ballistic-like" as we have seen in Fig. 2.

B. Correlation of the maximal transmission channel with quasinormal modes

To understand how the maximal transmission channel is formed and how it is modified by absorption, we investigate the related quasinormal modes. Unlike the input or output singular vectors of the transmission matrix, the quasinormal modes of an open random system are not orthogonal [48–50], thus it is difficult to decompose the 2D field pattern of a transmission eigenchannel by the quasinormal modes. Alternatively, we
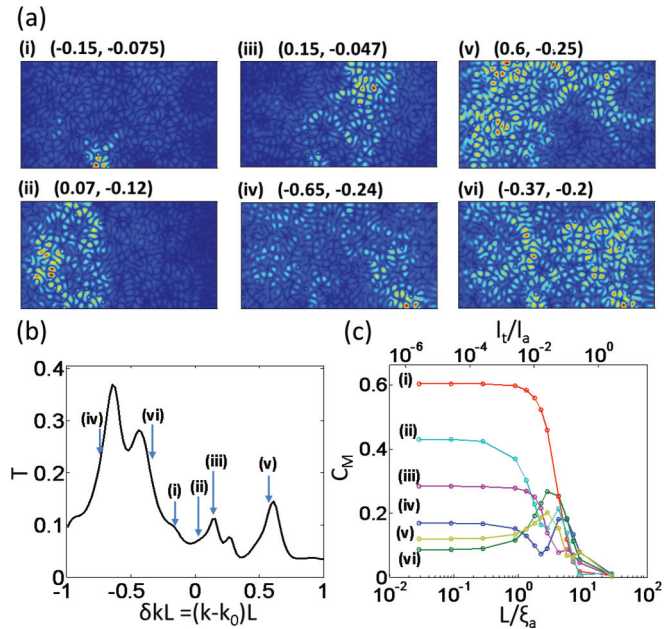
(a)

(b)

(c)

FIG. 4. (Color online) Quasinormal modes contributing to the maximal transmission channel. (a) Spatial distribution of electric field amplitude ($|E_z|$) for the six quasinormal modes with the highest degree of correlation with the maximal transmission channel in Fig. 2. The normalized center frequency $\delta k_r L = (k_r - k_o)L$ and linewidth $k_i L$ of each mode are given on top of each panel within parentheses $(\delta k_r L, k_i L)$, where $(k_r + i k_i)c = \omega_r + i\omega_i$ is the complex frequency of the quasimode at zero absorption. (b) A typical transmission spectrum for a random input field. The arrows mark the center frequency of the modes (i)–(vi). (c) Correlation of the six quasimodes, labeled (i)–(vi) in (a), with the maximal transmission channel C_M as a function of L/ξ_a. Modes that contribute the most at low absorption are closest to the channel frequency but spatially confined in the random structure so maximal transmission is facilitated through resonances hopping.

compute the degree of correlation between each quasimode and the eigenchannel to identify the modes that contribute significantly to the transmission channel. We used the commercial program COMSOL to compute the complex frequency ($\omega = \omega_r + i\omega_i$) and field pattern of each quasinormal mode in the disordered waveguide. The imaginary part ω_i of the complex frequency gives the decay rate or spectral width of the resonance, and the ratio of ω_r to ω_i is proportional to the quality factor. The contribution of a mode to the maximal transmission channel is reflected in the correlation of their spatial field profiles, $C_M = |\int E_q^*(x,y)E_c(x,y)dxdy|$, where $E_q(x,y)$ and $E_c(x,y)$ represent the normalized spatial distribution of the electric field E_z for the mode and the channel, respectively.

For the maximal transmission channel in Fig. 2, we identify six quasimodes with the highest degrees of correlation, and present their field patterns in Fig. 4 (a). The first three modes, labeled (i)–(iii), have the dominant contributions to the maximal transmission channel at zero absorption. Mode (i) is a tightly confined mode, which is visible in the field profile of the eigenchannel [Fig. 2(a)]. Modes (ii) and (iii) are more extended, but they are not spread over the entire system, instead mode (ii) concentrates in the left half of the disordered waveguide, and mode (iii) in the right half. Their

field patterns can be recognized in that of the eigenchannel. In contrast, modes (iv)–(vi) are spatially extended over an entire disordered waveguide, and their linewidths (decay rates) are larger than those of modes (i)–(iii). Figure 4(b) plots a typical transmission spectrum for a random input field. Modes (i)–(iii) are closest to the probe frequency and they have the largest contributions to the maximal transmission channel. Since these modes have little spatial overlap, optimum transport of energy is facilitated by hopping through them. Hence, the maximal transmission channel can be regarded as a necklace of resonances strung from one side of the system to the other. It is similar to the necklace state that dominates the transport in the localization regime [30], except that it is not a single state (quasinormal mode) but an eigenchannel of the transmission matrix. Although the total transmission at the center frequency of mode (ii) is lower than that of mode (v), mode (v) is spectrally farther away from the probe frequency than modes (ii), and its contribution to the maximal transmission channel is much smaller. We note that if the probe frequency shifts to the vicinity of the center frequency of mode (v), this mode will dominate the highest transmission channel, and the maximal energy transport occurs via an extended mode. Thus the necklace-like channels of maximal transmission exist only at certain probe frequencies.

Figure 4(c) shows how the correlation between the maximal transmission channel and the quasinormal modes change with absorption. In the regime of weak absorption ($L < \xi_a$), the correlation with each mode remains nearly constant, thus the field pattern of the transmission channel hardly changes. Note that the absorption is uniform and does not modify the spatial profile of individual quasimodes. When the absorption is strong ($L > \xi_a$), the correlation with modes (i)–(iii) decreases while the correlation with modes (v) and (vi) increases. These modes, unlike modes (i)–(iii), are extended over the entire system, and their contributions to the maximal transmission channel increase with absorption. With a further increase of absorption to $L/\xi_a = 9$, the maximal transmission channel has contributions from all the quasimodes that have spectral overlap with the channel. The interference of these modes leads to the formation of the ballistic-like channel with maximal transmission.

C. Scaling of spectral width of maximal transmission channel with absorption

The profile of the maximal transmission channel changes with frequency. Its spectral width gives the frequency interval over which a fixed input wavefront, optimized at a single frequency, still leads to strongly enhanced transmission. A previous study on light focusing through lossless turbid media shows that the frequency bandwidth of a wavefront optimized for a single focus is equal to the width of the speckle correlation function D/L^2, where D is the diffusion coefficient [51]. In this section, we investigate how absorption modifies the frequency bandwidth of the maximal transmission channel.

To compute the bandwidth, we first input monochromatic light at frequency k_0 with the wavefront corresponding to the input singular vector of the maximal transmission channel, and calculate the total transmission $T(k_0)$ at the output end. Then, we scan the input light frequency k while keeping the

same wavefront and calculate the new transmission value $T(k)$. As the frequency k is detuned from k_0, the total transmission T decreases. The bandwidth of the transmission channel is defined by the full width at half maximum (FWHM) as $\Delta k = k_2 - k_1$, where $T(k_1) = T(k_2) = T(k_0)/2$, $k_1 < k_0 < k_2$. With the introduction of absorption, Δk increases.

We observe varying scaling of Δk with l_t/l_a for various disorder configurations. Figure 5 (a) shows three types of behavior where the bandwidth increases linearly for realization A (blue dashed line), sublinearly for realization B (green solid line), and superlinearly for realization C (red dotted line) with l_t/l_a. In contrast, all the quasinormal modes exhibit the same linear increase of their spectral width with absorption. The average spectral width of quasimodes is shown by the black dash-dotted line in Fig. 5(a).

To interpret these results, we again consider the quasinormal modes underlying the transmission eigenchannel. We calculate the mode participation number defined as $M_{\rm eff} \equiv (\sum C_M)^2/(\sum C_M^2)$. The summation includes modes within a fixed frequency range of $|k - k_0|L < 0.62$. Modes with a frequency beyond this range have a negligible contribution as they are spectrally located far outside the bandwidth of the maximal transmission channel. Figure 5(b) plots the mode participation number vs absorption for the three realizations A, B, and C. For A (linear scaling of Δk with l_t/l_a), $M_{\rm eff}$ increases slightly with l_t/l_a, whereas for B (sublinear scaling of Δk with l_t/l_a), $M_{\rm eff}$ decreases. In contrast, C, which features a superlinear scaling of Δk with l_t/l_a, exhibits a rapid increase in $M_{\rm eff}$ as absorption increases. These results indicate that the bandwidth of the maximal transmission channel is related to the number of quasimodes contributing to the transmission. Figures 5(c) and 5(d) show the total transmission for the input vector that gives the maximal transmission at k_0 vs the frequency detuning of input light $k - k_0$ at $l_t/l_a = 0$ and 0.016 for realizations B and C, respectively. We note that without absorption, the transmission of B that possesses a higher mode participation number, has a broader bandwidth than C. This is explained by the fact that more modes at different frequencies contribute to the total transmission. The dramatic increase in the mode participation number for C adds to the absorption-induced broadening, leading to a superlinear increase of the channel bandwidth. Conversely, for B the broadening due to the increase of absorption is partially compensated by the reduction in the number of modes participating in the transmission, resulting in a sublinear behavior.

We have calculated many realizations, and found the behavior of A and C to be more common. To explain the trend of B in Fig. 5(b), we plot in Fig. 5(e) the correlations of the maximal transmission channel with six quasimodes, labeled (i)–(vi), in the disordered waveguide B. These modes have the highest correlations with the maximal transmission channel at zero absorption. The center frequencies of these modes are marked by arrows in Fig. 5(c), and their linewidths are given in Fig. 5(e). With increasing absorption, mode (vi) quickly de-correlates with the maximal transmission channel, indicating its contribution to the channel decreases rapidly. This mode is located close to the probe frequency and its linewidth is small without absorption. As shown schematically in Fig. 5(f), absorption spectrally broadens this mode, and
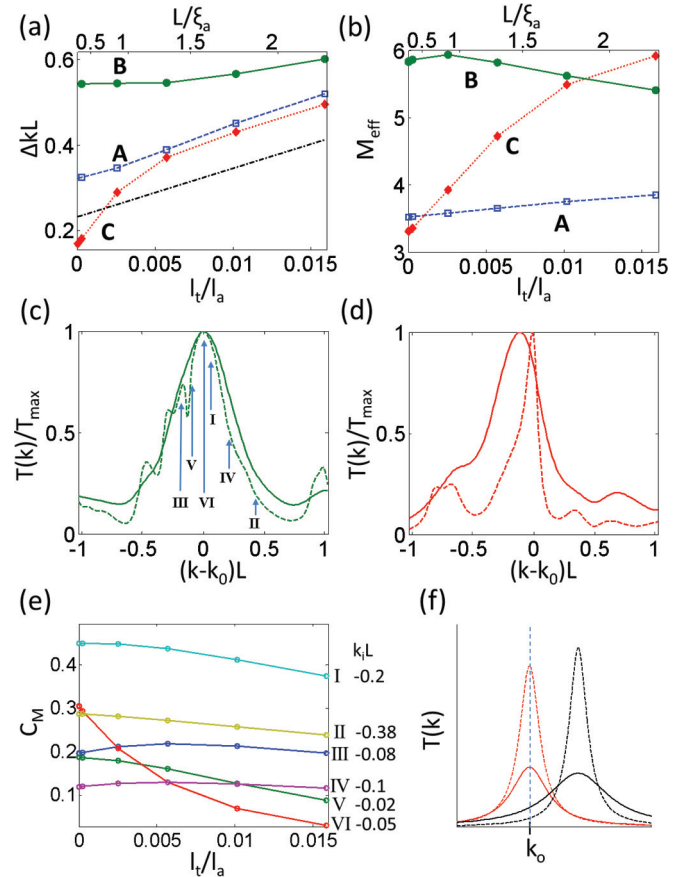

FIG. 5. (Color online) Dependence of the spectral width of the maximal transmission channel on absorption. (a) Spectral width of the maximal transmission channel Δk with absorption (bottom axis l_t/l_a, top axis L/ξ_a) for three waveguide realizations A, B, and C. The increase is linear for realization A (open squares connected by blue dashed line), sublinear for B (solid circles connected by green solid line), and superlinear for C (solid diamonds with red dotted line). Black dash-dotted line represents the average linewidth for the quasimodes. (b) Mode participation number $M_{\rm eff}$ vs absorption, it increases slightly for A, decreases for B, and increases dramatically for C. (c) and (d) Total transmission for the input vector that gives the maximal transmission at k_0 as a function of frequency detuning of input light $k - k_0$ at $l_t/l_a = 0$ (dashed line) and 0.016 (solid line) for realizations B and C. (e) Correlation of six quasimodes, labeled (i)–(vi), with the maximal transmission channel as a function of l_t/l_a. The normalized center frequency of each mode is marked by an arrow in (c), and the normalized linewidth k_iL at zero absorption is given next to the panel. (f) Schematic of the transmission spectrum having two quasimodes in the absence of absorption (dashed line) and with absorption (solid line). It shows how the spectral broadening by absorption modifies the contributions of these two modes to the transmission channel at k_0. For the mode centered at k_0, its contribution to the channel decreases rapidly. For the mode farther away from the probe frequency, its contribution increases when absorption becomes strong.

its spectral overlap with the channel decreases, leading to a reduction in its contribution to the maximal transmission channel. Another mode (v) which has narrower linewidth than mode (vi) is detuned from the probe frequency, and its spectral overlap with the channel is lower. Consequently

its contribution only decreases slightly with absorption. All other modes have broader linewidth at zero absorption, and the absorption-induced broadening is relatively weak. Thus their contributions to the maximal transmission channel change more slowly with absorption. Therefore, the decrease of mode participation number with absorption is due to rapid reduction in contributions from the long-lived modes that are almost in resonance with the channel. With a further increase of absorption, the modes, initially having little overlap with the probe frequency, are spectrally broadened enough to contribute to the maximal transmission channel at the probe frequency, leading to an increase of the mode participation number.

Even though there appears to be different scaling behavior from one disorder realization to another, the ensemble-averaged bandwidth of the maximal transmission channel increases linearly with absorption. This result echoes the finding reported in Ref. [40] where the linewidth of the perfect absorption channel exhibits a linear scaling with absorption.

IV. MINIMAL REFLECTION CHANNEL

In lossless random media, the maximal transmission channel is equivalent to the minimal reflection channel; the only way of reducing reflection is to enhance transmission. In an absorbing medium, this is no longer true: Reflection may be reduced by enhancing absorption instead of transmission. In this section, we study the relations between the maximal transmission channel, the minimal reflection channel, and the maximal absorption channel in absorbing random media.

The reflection eigenchannels are obtained by singular value decomposition of the field reflection matrix r. The input singular vector corresponding to the lowest singular value gives the minimal reflectance. We compute the correlation between the input singular vector for maximal transmission and that for minimal reflection using the same definition as in Eq. (2) and present the result in Fig. 6 (blue solid line). The correlation is almost one in the weak absorption regime $(L < \xi_a)$, but drops quickly once in the strong absorption regime $(L > \xi_a)$. When the absorption is weak, the lowest reflection is still achieved by maximizing transmission. With strong absorption, light that is not reflected can be either transmitted or absorbed. Hence, reflection is reduced by enhancing both transmission and absorption.

To find the maximal absorption channel, we introduce the matrix h that links light incident from one end of the waveguide to the transmitted and reflected fields:

$$h = \begin{pmatrix} r \\ t \end{pmatrix}, \qquad (3)$$

where r and t are the field reflection and transmission matrices. An eigenvalue of $h^\dagger h$ represents the sum of the reflectance and the transmittance of its associated input singular vector. The singular vector of h with the smallest singular value corresponds to the maximal absorption channel. The correlation coefficient between the minimal reflection and maximal absorption channels is plotted as a function of the absorption in Fig. 6 (black dashed line). As the correlation between the minimal reflection channel and the maximal transmission channel decreases, the correlation between the minimal reflection channel and the maximal absorption channel
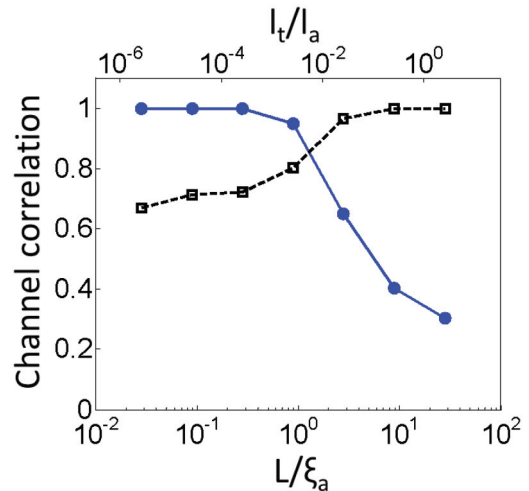

FIG. 6. (Color online) Absorption-induced change of minimal reflection channel. Solid circles connected by solid line represent the correlation between the minimal reflection channel and the maximal transmission channel. Open squares connected by dashed line represent the correlation between the minimal reflection channel and the maximal absorption channel. The minimal reflection channel is the same as the maximal transmission channel when absorption is weak $L < \xi_a$, but it approaches the maximal absorption channel as absorption is strong $L > \xi_a$.

increases. Eventually, in the strong absorption regime, the minimal reflection channel becomes identical to the maximal absorption channel, indicating that the minimal reflection is achieved by maximizing absorption instead of transmission.

Intuitively one expects all reflection eigenvalues to decrease with increasing absorption. Indeed, we show in Fig. 7(a), the ensemble-averaged minimal reflection eigenvalue decreases with absorption. Strikingly, in a significant number of realizations we have observed the opposite behavior, a counterintuitive increase of reflection caused by absorption. In Fig. 7(a) we show the minimal reflectance of a selected realization. The minimal reflectance (eigenvalue of $r^\dagger r$) first decreases slightly as L/ξ_a increases from 0 to 1, then rises rapidly by a factor of 3 before dropping again at larger absorption. In Figs. 7(b) and 7(c) we show the electric field patterns inside the random waveguide corresponding to the minimal reflectance without absorption and at $L/\xi_a = 3$ where the lowest reflection eigenvalule reaches a local maximum. In the absence of absorption, light penetrates deep into the random medium with the field maxima close to the center of the sample. However, at $L/\xi_a = 3$, the penetration depth is greatly reduced and the field maxima shift to the input end of the random system. The field pattern close to the input surface of the same is also strongly modified.

To understand this counterintuitive behavior, we investigate the quasimodes that contribute to the minimal reflection channel. Figure 7(d) plots the degree of correlation between the minimal reflection channel and two quasimodes (labeled 1 and 2) that have the highest contributions, and Figs. 7(e) and 7(f) show their field patterns. Without absorption, the least reflection channel is dominated by mode 1 that is located near the center of the sample. Destructive interference of
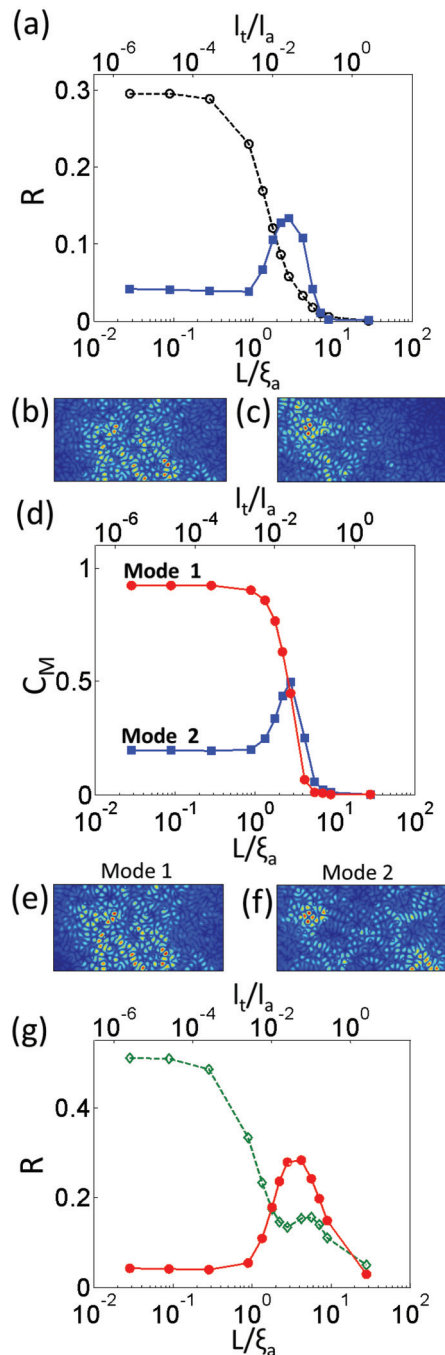
FIG. 7. (Color online) Example of increasing minimal reflectance with absorption. (a) Open circles connected by dashed line represent the ensemble-averaged lowest reflection eigenvalue as a function of absorption. Solid squares connected by solid line represent the lowest reflection eigenvalue of a selected realization that increases with absorption. (b)–(g) are for the selected realization. (b) and (c) Spatial distribution of the electric field amplitude $|E_z(x,y)|$ inside the random waveguide at $L/\xi_a = 0$ and 3, respectively. The lowest reflection eigenvalue reaches a local maximum at $L/\xi = 3$. (d) Correlation of the minimal reflection channel with quasimodes 1 and 2. (e) and (f) Electric field patterns of mode 1 and 2. (g) Solid circles connected by solid line (open diamonds connected by dashed line) represent the reflectance of a fixed input wavefront $E_1(E_2)$ that corresponds to the input singular vector of the minimal reflection channel at $L/\xi_a = 0$ ($L/\xi_a = 3$).

various scattering paths of light in the disordered waveguide minimizes the reflectance. This explains the low minimal reflectance value of the selected realization compared to the ensemble-averaged one. With the introduction of absorption to the system, relative amplitudes of these paths are changed, the longer paths are attenuated more than the shorter paths, thus the destructive interference is weakened, leading to an increase of the reflectance as shown in Fig. 7(a). When the minimal reflectance has a maximum at $L/\xi_a = 3$, the field pattern of the minimal reflection channel shown in Fig. 7(c), resembles that of mode 2 in the left half of the waveguide. At this strong absorption level, the contribution of mode 1 to the minimal reflection channel is negligible, whereas mode 2 becomes dominant, which is a mode with a larger overlap with the input light into the disordered waveguide. Therefore, the interference in the bulk of the sample—which is the cause of open transmission channels—is suppressed, which leads to an increased reflectance.

Let us now consider the input wavefront E_1, which corresponds to the minimal reflection channel (or maximal transmission channel) without absorption. E_1 couples most of the input energy into mode 1. Figure 7(g) shows the reflectance associated with input wavefront E_1 as a function of absorption L/ξ_a. When absorption becomes significant ($L > \xi_a$), the reflectance increases rapidly, up to 5 times its value at $L/\xi_a = 0$. Another input wavefront E_2, corresponding to the minimal reflection channel at $L/\xi_a = 3$, couples most of the energy into mode 2. In Fig. 7(g), we show the evolution of the reflection value associated to this wavefront with absorption. As expected, the reflectance decreases with increasing absorption. Once the reflectance with input wavefront E_2 becomes lower than that associated with E_1, mode 2 becomes dominant in the minimal reflection channel. This illustrates that with increasing absorption, the mechanism that produces the minimal reflection channel changes from transmission to bulk absorption. Moreover, it shows the significant role played by interference of scattered waves up to the point where the absorption becomes dominant.

V. DISCUSSION

It has been suggested that the change in transport behavior of the maximal transmission channel with increasing absorption bears similarity to the change found recently in the dynamic transport of localized samples [52]. There ballistic transport was observed at early times after a pulsed excitation, which involved all excited quasimodes. At later times, the modes with shorter lifetimes dissipate, and only the modes with longer lifetimes survive and dominate transmission. In the case of strong absorption, long optical paths are eliminated and only short paths survive, making the transport ballistic-like. The maximal transmission channel consists of both long-lived and short-lived modes, similar to the dynamic transport at early times. In the long time limit, the transmission of a localized sample is dominated by a single quasimode with the longest lifetime, however, the maximal transmission channel in a diffusive sample with weak or no absorption consists of multiple long-lived modes as shown in Sec. III.

It is worth noting that such necklace-like transport due to hopping of several spatially confined modes is unlikely to

exist if the width of the disordered waveguide is increased significantly. This is because the localization length, which increases linearly with the waveguide width, will become much larger than the system length. Hence the system moves farther away from the localization regime; most quasimodes are spatially extended over the random media. In addition, the mode density increases with the system size. No matter what the probe frequency is, there are always extended modes nearby which contribute significantly to the transmission channel. Thus the maximal transmission channel is expected to consist of many extended modes whose interference leads to the highest transmission. Only in the diffusive system close to localization transition, some of the quasimodes become spatially confined, and the maximal transmission channel can be necklace-like.

The ballistic-like maximal transmission channel, found here in the presence of strong absorption, may enable new modes of imaging that are specific to absorbing media. To check whether such ballistic-like transmission channels also exist without absorption, we examine all transmission channels in the nonabsorbing disordered waveguides. We compute the histogram of the Poynting vector direction $P(\theta_s)$ for every transmission eigenchannel in three random realizations. The variance of $P(\theta_s)$ remains large for all transmission eigenchannels, including those with low transmission eigenvalues. Hence, the ballistic-like transmission channel does not seem to exist in our systems without absorption. Nevertheless, it is important to introduce a physical quantitative that measures how "ballistic" a transmission channel is. One possibility is the average transmission time [53], which merits further study.

VI. CONCLUSION

We have performed a detailed numerical study to understand how absorption modifies transport in a 2D disordered waveguide, with emphasis on the maximum transmission channel. The maximal transmission channel is relatively robust against absorption compared to the transmittance. Its input wavefront remains nearly unchanged up to $L \approx \xi_a$, but changes rapidly beyond that point. In the maximal transmission channel, light propagates through the random structure along winding paths when absorption is weak ($L < \xi_a$), and takes more straight routes once absorption is significant ($L > \xi_a$). We investigate the correlations between the quasinormal modes and the maximal transmission channel to illustrate the mechanism of enhanced transmission in both weak and strong absorption regimes. Maximal transmission is facilitated by hopping through localized modes when absorption is weak, and is dominated by more extended modes when absorption is strong. We observe distinct scaling behavior for the spectral width of the maximal transmission channel in different random configurations. Such differences result from the absorption-induced change in the number of quasimodes that participate in the maximal transmission channel. The channel spectral width increases linearly with absorption, if the mode participation number M_{eff} remains almost constant; the width increases sublinearly if M_{eff} decreases, and superlinearly if M_{eff} increases.

In the absence of absorption, minimal reflection corresponds to maximal transmission, but this correspondence no longer holds in the regime of strong absorption ($L > \xi_a$), where minimal reflection corresponds to enhanced absorption. In some instances, we have observed the surprising feature that the minimal reflection eigenvalue increases with absorption, which can be explained by the reduction of destructive interference. The numerical study presented here provides a physical understanding of the effects of absorption on transmission and reflection eigenchannels at the relevant mesoscopic scale, which will hopefully serve in the interpretation of experimental work, and in the design of practical applications.

[1] M. P. Van Albada and A. Lagendijk, Phys. Rev. Lett. **55**, 2692 (1985).

[2] P.-E. Wolf and G. Maret, Phys. Rev. Lett. **55**, 2696 (1985).

[3] B. L. Altshuler, A. P. Lee, and R. A. Webb, *Mesoscopic Phenomena in Solids* (North Holland, Amsterdam, 1991).

[4] F. Scheffold and G. Maret, Phys. Rev. Lett. **81**, 5800 (1998).

[5] E. Akkermans and G. Montambaux, *Mesoscopic Physics of Electrons and Photons* (Cambridge University Press, Cambridge, 2007).

[6] A. Lagendijk, B. van Tiggelen, and D. S. Wiersma, Phys. Today **62**, 24 (2009).

[7] I. M. Vellekoop and A. P. Mosk, Phys. Rev. Lett. **101**, 120601 (2008).

[8] J. B. Pendry, Physics **1**, 20 (2008).

[9] W. Choi, A. P. Mosk, Q.-H. Park, and W. Choi, Phys. Rev. B **83**, 134207 (2011).

[10] W. Choi, Q. H. Park, and W. Choi, Opt. Express **20**, 20721 (2012).

[11] Z. Shi and A. Z. Genack, Phys. Rev. Lett. **108**, 043901 (2012).

[12] M. Kim, Y. Choi, C. Yoon, W. Choi, J. Kim, Q.-H. Park, and W. Choi, Nat. Photon. **6**, 581 (2012).

[13] M. Davy, Z. Shi, J. Wang, and A. Z. Genack, Opt. Express **21**, 10367 (2013).

[14] S. M. Popoff, A. Goetschy, S. F. Liew, A. D. Stone, and H. Cao, Phys. Rev. Lett. **112**, 133903 (2014).

[15] O. N. Dorokhov, Solid State Commun. **44**, 915 (1982).

[16] O. N. Dorokhov, Solid State Commun. **51**, 381 (1984).

[17] P. A. Mello, P. Pereyra, and N. Kumar, Ann. Phys. **181**, 290 (1988).

[18] Y. V. Nazarov, Phys. Rev. Lett. **73**, 134 (1994).

[19] I. M. Vellekoop and A. P. Mosk, Opt. Lett. **32**, 2309 (2007).

[20] Z. Yaqoob, D. Psaltis, M. S. Feld, and C. Yang, Nat. Photon. **2**, 110 (2008).

[21] S. M. Popoff, G. Lerosey, R. Carminati, M. Fink, A. C. Boccara, and S. Gigan, Phys. Rev. Lett. **104**, 100601 (2010).

[22] I. M. Vellekoop, A. Lagendijk, and A. P. Mosk, Nat. Photon. **4**, 320 (2010).

[23] S. Popoff, G. Lerosey, M. Fink, A. C. Boccara, and S. Gigan, Nat. Commun. **1**, 1 (2010).

[24] W. L. Vos, T. W. Tukker, A. P. Mosk, A. Lagendijk, and W. L. IJzerman, Appl. Opt. **52**, 2602 (2013).

[25] M. Kim, W. Choi, C. Yoon, G. H. Kim, and W. Choi, Opt. Lett. **38**, 2994 (2013).

[26] W. Choi, M. Kim, D. Kim, C. Yoon, C. Fang-Yen, Q. Park, and W. Choi, arXiv:1308.6558.

[27] J. Wang and A. Z. Genack, Nature (London) **471**, 345 (2011).

[28] J. Wang, Z. Shi, M. Davy, and A. Z. Genack, Int. J. Mod. Phys. Conf. Ser. **11**, 1 (2012).

[29] J. B. Pendry, J. Phys. C **20**, 733 (1987).

[30] J. B. Pendry, Adv. Phys. **43**, 461 (1994).

[31] J. Bertolotti, S. Gottardo, D. S. Wiersma, M. Ghulinyan, and L. Pavesi, Phys. Rev. Lett. **94**, 113903 (2005).

[32] P. Sebbah, B. Hu, J. M. Klosner, and A. Z. Genack, Phys. Rev. Lett. **96**, 183902 (2006).

[33] K. Y. Bliokh, Y. P. Bliokh, V. Freilikher, A. Z. Genack, B. Hu, and P. Sebbah, Phys. Rev. Lett. **97**, 243904 (2006).

[34] K. Y. Bliokh, Y. P. Bliokh, V. Freilikher, A. Z. Genack, and P. Sebbah, Phys. Rev. Lett. **101**, 133901 (2008).

[35] P. W. Brouwer, Phys. Rev. B **57**, 10526 (1998).

[36] A. G. Yamilov and B. Payne, Opt. Express **21**, 11688 (2013).

[37] A. A. Chabanov, M. Stoytchev, and A. Z. Genack, Nature (London) **404**, 850 (2000).

[38] Y. D. Chong, L. Ge, H. Cao, and A. D. Stone, Phys. Rev. Lett. **105**, 053901 (2010).

[39] W. Wan, Y. D. Chong, L. Ge, H. Noh, A. D. Stone, and H. Cao, Science **331**, 889 (2011).

[40] Y. D. Chong and A. D. Stone, Phys. Rev. Lett. **107**, 163901 (2011).

[41] M. Grätzel, J. Photochem. Photobiol. C. **4**, 145 (2003).

[42] A. Hagfeldt, G. Boschloo, L. Sun, L. Kloo, and H. Pettersson, Chem. Rev. **110**, 6595 (2010).

[43] M. Kim, W. Choi, C. Yoon, G. H. Kim, S. Kim, G. Yi, Q. Park, and W. Choi, arXiv:1308.6553.

[44] J. D. Joannopoulos, S. Johnson, J. Winn, and R. Meade, *Photonic Crystals: Molding the Flow of Light* (Princeton University Press, Princeton, 2008).

[45] http://www.comsol.com.

[46] M. C. W. van Rossum and T. M. Nieuwenhuizen, Rev. Mod. Phys. **71**, 313 (1999).

[47] X. Wu, J. Andreasen, H. Cao, and A. Yamilov, J. Opt. Soc. Am. B **24**, A26 (2007).

[48] P. T. Leung, S. S. Tong, and K. Young, J. Phys. A **30**, 2139 (1997).

[49] P. T. Leung, S. S. Tong, and K. Young, J. Phys. A **30**, 2153 (1997).

[50] E. S. C. Ching, P. T. Leung, A. Maassen van den Brink, W. M. Suen, S. S. Tong, and K. Young, Rev. Mod. Phys. **70**, 1545 (1998).

[51] F. van Beijnum, E. G. van Putten, A. Lagendijk, and A. P. Mosk, Opt. Lett. **36**, 373 (2011).

[52] J. Wang, A. A. Chabanov, D. Y. Lu, Z. Q. Zhang, and A. Z. Genack, Phys. Rev. B **81**, 241101(R) (2010).

[53] S. Rotter, P. Ambichl, and F. Libisch, Phys. Rev. Lett. **106**, 120602 (2011).